IMPLICATIONS OF THE STRONG-MOTION RECORDS FROM A RETROFITTED CURVED BRIDGE ON SEISMIC DESIGN AND PERFORMANCE

W.D. Liu, A. Kartoum, S. Dhillon, X. Chen, R.A. Imbsen
Imbsen & Associates, Inc.
Sacramento, California

ABSTRACT

Structural responses recorded during three recent earthquakes (1992 Landers and Big Bear and 1994 Northridge) were used to evaluate the performance of the retrofitted single column viaduct (Route 10/215 Interchange in Colton). The column deformation experienced range from low in the Northridge earthquake up to about 70% yield deformation level during the Landers earthquake. These results were compared with the deformation-based design practice for column retrofit. Effect of foundation contribution was also compared with the design practice. Results from this study support the successful performance of other similarly retrofitted bridges during the Northridge earthquake.

INTRODUCTION

While most post-earthquake investigations focus on the structure failure, it is equally important to identify and verify the effectiveness of successful design schemes which meet the desired seismic performance goal. The connector interchange structures are typically very important structures because of their strategic location in the urban transportation network. Therefore, these bridges have been given priority for seismic upgrading.

The June 28, 1992, Landers and Big Bear earthquakes with magnitudes, M_s, 7.5 and 6.6, respectively, were among the largest magnitude earthquakes recorded in the United States. This was the first time that a major curved bridge was monitored during a strong earthquake. More importantly, this was the first time that a bridge, retrofitted with steel confinement casings around columns, was monitored during a strong earthquake.

During the January 17, 1994, Northridge earthquake (Magnitude M_w 6.7), the highway bridge structures in the Los Angeles area suffered significant damage. Among these damaged structures, two curved viaducts in the Route 14/5 Interchange suffered partial collapse. These are single column viaducts designed and constructed in the early 1970s which had not been retrofitted for column deficiencies.

A similar curved, single column viaduct structure, the Route 405/10 Interchange, survived the strong ground shaking. This bridge is about 15 miles south of the epicenter, four miles west of the collapse section on I10 and five miles east of a Santa Monica site where horizontal ground motion up to 0.93 g was recorded. Regardless

of the close proximity to the epicenter and the expected strong shaking, the bridge suffered only the toppling of rocker bearings at the abutment. The instrument on the bridge recorded a peak vertical acceleration of 1.83 g. The peak horizontal motions recorded were 1.0 g at the west abutment and 0.52 g (transverse) at top of Bent 9. Other than the bearing damage, the bridge did not suffer any noticeable damage. The satisfactory performance of this bridge was attributed to the retrofit scheme used for the columns and the footings. Unfortunately, the instrumentation on this bridge is not sufficient to conduct more detailed performance assessment.

These two bridges are geometrically similar to the fully instrumented interchange in Colton. To establish an important benchmark, the Route 10/215 Interchange and the recorded ground motions during the past three earthquakes are used in this study. The emphasis is on the behavior of the retrofitted single column bent, and how they compare with current design practice using a deformation-based design methodology. In addition to the column performance, a detailed evaluation of the fully instrumented Bent 8 allows an assessment of the foundation effect and correlation with current design practice for calculation of foundation stiffness. The overall dynamic characteristics of the bridge have also been determined based on measurements to allow a comparison with the analytical model prediction.

To account for the expected pounding effect at the span hinges, a procedure based on the restitution coefficient approach is proposed to account for energy loss.

A previous study by Fenves & Desroches (1995) focused on the global response correlation with the analytical model. In this paper, we will focus on the seismic performance and implication to the design practice.

DESCRIPTION OF THE BRIDGE

The Route 10/215 Interchange is located near the city of Colton, in San Bernardino County, California. The interchange is comprised of several bridges, including the NW Connector Overcrossing that connects eastbound Route 10 from Los Angeles to northbound Route 215 to San Bernardino. This bridge has been instrumented to monitor seismic performance by the California Division of Mines and Geology as part of its Strong Motion Instrumentation Program (CSMIP).

The NW Connector Overcrossing is a curved, cast-in-place, concrete box girder bridge, as shown in Figure 1. The alignment of the bridge consists of a compound curve having radii of 1200 feet and 1300 feet. There are 16 spans, having a total length of 2540 feet and width of 41 feet. The superstructure has five intermediate span hinges to accommodate movements and to separate post-tensioned concrete spans from conventionally reinforced spans. The bridge substructure is comprised of monolithic abutments and single column bents. The columns are 5.5 feet by 8.0 feet flared octagonal shaped. The foundations consist of pile footings with 70 ton driven concrete piles at the abutments and bents, except for Bent 2 which has 100 ton piles. Both Bent 3 and Bent 8 are founded on footings with 36 piles.

The bridge was originally constructed in 1972 with several inherent seismic vulnerabilities that include: inadequate widely spaced ties in the columns, no top mat of reinforcement in the footings, and insufficient support length at the hinges. In 1991, the bridge was seismically retrofitted by placing steel jackets ($^1/_2$" thick) around columns, strengthening footings and abutments, and by installing new restrainers at the hinges. At 12 of the 15 bents, full-height jackets were provided and the footings were enlarged with driven steel piles provided to increase the moment capacity of the foundations. At Bents 8, 12 and 14, steel jackets were provided at the lower 18 feet above the footing, and the footings were not modified. Abutment catchers were provided to prevent drop-span failure if abutment backwall failed.

DESCRIPTION OF THE INSTRUMENTATION

A total of 34 sensors are used on the bridge, as shown in Figure 1. The maximum acceleration values observed in each sensor are summarized in Table 1 for the three earthquakes. Table 2 shows the sensor layout by individual frames.

The instrumentation layout plan was carefully thought out with the following features:

a. Each frame was instrumented with at least three sensors (one longitudinal and two transverse). This allows a complete characterization of the lower horizontal modes of each frame.

b. The instrumentation at Bent 8 includes four sensors at the foundation and four sensors at the deck. This provides a unique opportunity to study in detail the transverse response of the bent including:

   - the effect of soil-structure interaction at the base;
   - the effect of the rotational support input motion;
   - the effective stiffness property (i.e., moment of inertia) of the retrofitted column; and
   - the modeling assumptions typically used for the single column bent.

   Similar bent transverse study can also be conducted for Bent 3.

c. The instrumentation on Span 7 includes four vertical sensors to quantify the vertical and torsional vibration of the cantilever deck segment.

d. Across each expansion joint (span hinge), there is at least two transverse sensors. In four hinges, longitudinal sensors are also used. Given the longitudinally restrained boundary conditions at both abutments, these pairs of sensors at hinges can be studied to establish the sequence of impacting occurred.

The free-field ground motions are recorded in the nearby CSMIP Station 23542. However, they are not synchronized with the sensors on the structure.

Strong-Motion Data – Free Field Motions

The three-component free-filed motions were rotated to the longitudinal (tangential) and transverse directions at Bent 8. The 5% damped response spectra are calculated. The spectral accelerations for these three vibration periods are summarized in Table 3. In the transverse direction, the Landers earthquake is much higher for periods greater than 1.5 sec. For intermediate period range between 0.4 to 0.8 sec., the Northridge earthquake is much stronger than the others.

Strong-motion data for the superstructure deck with and without the high frequency spikes were reported by Huang & Shakal (1995) for the Landers and Big Bear earthquakes. It is inferred that the spikes were generated by the impact between adjacent deck sections across the span hinges. (Malhotra, et al, 1994)

RESPONSE INTERPRETATION OF BENT 8

The pile supported single column bent is instrumented with eight sensors: four on the deck level and four on the footing level. To facilitate interpretation, the transverse response of the bent structure is idealized as a three degrees of freedom system: translation of the deck and translation and rotation of the pile cap, as shown in Figure 2.

Analytical Formulation

The total motion at the bent cap is composed of two components: column deformation u, and the foundation contribution $\bar{u}$ which can be defined as follows:

$$u^t(t) = \bar{u}(t) + u(t) \tag{1}$$

$$\bar{u}(t) = u_o(t) + L\,\theta_o(t) \tag{2}$$

where L is the height to the C.G. of the deck. Given the foundation stiffness coefficients for the translational and rotational degrees of freedom, k_u and k_θ, the effective foundation stiffness is defined as:

$$\bar{k} = \left(\frac{1}{k_u} + \frac{L^2}{k_\theta} \right)^{-1} \tag{3}$$

This is schematically shown in Figure 2(d). The total lateral stiffness of the bent including the foundation contribution is:

$$K_{eff} = k\left(1 + \frac{k}{\bar{k}} \right)^{-1} \tag{4}$$

This is shown in Figure 2(e). This allows a systematic evaluation of the column behavior and the foundation effect.

Column Behavior Characteristics

By eliminating the foundation contribution, $\bar{u}$, the measured response data can be used to quantify the behavior characteristics of the column, i.e., the column stiffness k, damping c, the fixed-base vibration frequency ω_{FB},

$$\omega_{FB} = \sqrt{k/m} \tag{5}$$

where m is the tributory mass of the superstructure. The equation of motion for the fixed-base bent is

$$m\ddot{u}^t + c\dot{u} + k\,u = o \tag{6}$$

or

$$\ddot{u}^t + 2\xi\omega_{FB}\dot{u} + \omega_{FB}^2\,u = o \tag{7}$$

Using measured time history response $\ddot{u}^t(t)$ at the deck (channel 20) and the derived column deformation time history u(t), the parameters ω_{FB} and ξ can be determined by the equivalent linearization technique.

Using this approach, the column properties were identified for the three earthquakes. This was done using the entire measured duration. The results are summarized in Table 4.

The column stiffness k is calculated based on the tributory weight of 2973 kip at Bent 8 (including the box-girder superstructure and half of the column weight). The normalized force-displacement hysteretic loops are shown in Figures 3(a) through 3(c) for the three earthquakes. The maximum column deformations vary from 5.6 inches for the Landers earthquake, 3.5 inches for the Big Bear earthquake, and 1.25 inches for the Northridge earthquake. These displacements cover a wide range. As shown in Table 4, the fixed-base vibration frequency and the effective linear stiffnesses of the column vary consistently with the amplitude.

To further evaluate the column behavior during these earthquakes, the response time histories were divided into 10 second duration windows. For each time window, the root-mean-squared (RMS) displacement and normalized force responses were calculated. These force-displacement pairs are shown in Figure 4 which shows clearly a nonlinear relationship. At the lower RMS displacement, the stiffness (as indicated by the slope) is much higher, and gradually softens as the RMS displacement reached 1.5" to 2.5" level.

Correlation with Analytical Capacity Prediction

In the current practice, a deformation-based design methodology is being promoted. For each critical cross section, the moment-curvature relationship is computed based on the nonlinear material constitutive relationships for concrete and steel reinforcement. The objective is to quantify the deformation capacity provided by the design reinforcement details, and to allow a judicious selection of design criteria (e.g. not to allow concrete strain beyond a certain level).

For the retrofitted column sections with partial height steel casing, it is important to quantify the increase in lateral stiffness. This is caused by the bond transfer between the original column and the steel shell and results in partial composite action. For flexural columns with aspect ratio around L/D = 6, laboratory test showed a modest increase of lateral stiffness by 10% to 15%. (Chai, 1996)

This can be accounted for in the component stiffness calculation. As shown in Figure 5, the effective moment of inertia varies along the column height. In the center portion of the encased region, the full composite action is possible to be developed. From there on to the ends of the casing, partial composite action exists.

For the Bent 8 column, several moment-curvature relationships were used for the upper unencased section (flared), the lower gapped zone, and the varying degrees of composite action. Using these results, the fixed-base column lateral force-deformation curve was developed, as shown in Figure 5(e). Based on the bilinear idealization, the column with steel casing retrofit will yield at a displacement level of about 3.5 inches. This compares reasonably well with the measured results, as shown in Figure 4.

The secant stiffness in the transverse direction corresponding to the yield of the steel reinforcement is 1630 kip/ft. This is consistent with the stiffnesses derived from the measured results because of the higher deformation level implied in the calculation, as shown in Figure 4.

Foundation Flexibility Effects

Based on available soil boring data, the standard procedures as summarized in the FHWA Report entitled *Foundation Design to Resist Earthquake Loads*, are used to calculate the pile group stiffness coefficients. For the transverse translation and the rotation about the longitudinal axis, the combined pile group and pile cap stiffnesses are:

$$k_u = 1.86 \times 10^5 \text{ kip/ft}; \; k_\theta = 7.22 \times 10^7 \text{ kip-ft/rad.}$$

The effective foundation stiffness as defined in Eq. (3) is

$$\bar{k} = 28{,}832 \text{ kip/ft}$$

It is of interest to note that the translation foundation stiffness contributes to only 15% of the total foundation effect on the bent cap displacement. For design purpose, the rocking effect of pile group foundation is more critical to the seismic response prediction.

As shown in Eq. (4), the foundation contribution to the bent cap displacement is determined by $(1+ k/\bar{k})$. These results are summarized in Table 4 for the three earthquakes. Based on these results, the overall transverse vibration frequency is only affected by 3% to 6% during these three earthquakes. The bent cap displacements during these three earthquakes were affected by 7% to 12% due to foundation flexibility. This compares very well with observed data.

MODELING REFINEMENT FOR SPAN HINGE IMPACT

The nonlinear behavior (cable stretching and deck impacting) across the span hinge is a critical feature of the overall bridge response under strong earthquake shaking. During the 1989 Loma Prieta earthquake, this has been observed in the Route 24/580/980 Interchange, a highly curved viaduct. (Liu, et al, 1994).

This deck impacting can also be seen in the transverse shear force hysterestic loop of the column. When the bridge moves outward (negative displacement), the adjacent span separates; when the bridge moves inward (with positive column displacement), the deck impact at the inside edge occurs and additional force develops. This is most clearly shown in Figure 3(b) for the Big Bear earthquake.

One of the critical issues has been how to model the stiffness characteristics and energy loss during impact. A usual practice is to use a very large elastic impact stiffness to prevent the overlapping of adjacent deck. However, this may result in the unusually high force. Kawashima and Penzien (1976) had conducted a correlation study with shake table testing of a curved bridge model. They recommended the use of an elastic impact stiffness which is ten times the axial stiffness of the deck. This will assure that the duration of impact is sufficiently short. However, no energy loss was considered.

The *coefficient-of-restitution* approach can be used to model the finite duration impact and energy loss. (Cross and Jones, 1993) In short, this impact restitution approach states that the relative separation velocity immediately after the impact, v_s, is a fraction of the relative approaching velocity before the impact, v_A :

$$v_s = e\, v_A \tag{8}$$

where

e = coefficient of restitution ($0 \le e \le 1$)
e = 1 perfect elastic rebound
e = o no impact

This is schematically shown in Figure 6. During the impact, the two adjacent sections stick together and the connection can be represented using an equivalent

spring-damper at the point of contact for the duration of impact. To assure the impact duration is short, the impact stiffness should be much greater (say ten times) than the structural stiffness.

For the given coefficient of restitution, it can be shown that the equivalent dashpot coefficient c_I during impact is

$$\xi_I = \frac{c_I}{c_{cr}} = 10.5 \frac{-\frac{\ln e}{\pi}}{\sqrt{1+\left(\frac{\ln e}{\pi}\right)^2}} \tag{9}$$

where c_{cr} is the critical damping of the structural frame. For various values of e, the equivalent dashpot can be determined. This approach allows the energy loss during impact to be taken into account in the analytical model.

GLOBAL DYNAMIC CHARACTERISTICS

Based on the measured responses at each frame, Fourier amplitude spectra were computed. These were used to identify the dominant frequencies, as shown in Figure 7. Using the cross power spectral density functions calculated relative to a fixed reference point in each frame, the phase angles were determined and the vibration mode shapes of the bridge can be portrayed.

Using the data collected during Landers earthquake, the first three modes are shown in Figure 8. Because of the noise in the data and the signal processing procedure, two very closely-spaced frequencies and shapes were determined for the first mode, as shown in the Figure. However, based on the distribution of substructure stiffnesses as reflected by the column heights, we believe there is only one mode indicated by the solid line in the Figure.

SUMMARY AND CONCLUSIONS

Data collected from three recent earthquakes at the I10/215 Interchange were utilized to evaluate the seismic performance including the component column behavior, foundation flexibility effect, overall structural periods, and mode shapes.

The most significant findings were that the behavior characteristics of the retrofitted columns can be predicted quite well using the deformation-based methodology. Since the response levels in these three earthquakes vary from low (Northridge earthquake) to high (Landers earthquake), these comparisons provided a valuable benchmark. As indicated in the measured data, columns were loaded well beyond cracking load and reached 70% of the calculated yield deformation.

The nonlinear force-deformation behavior was observed in the measured data which is very consistent with the analytical prediction. Because of the excellent correla-

tion, the expected seismic performance of the retrofitted column can be assured. Note that the peak transverse acceleration at top of Bent 8 was 0.39 g (Channel 20) and 0.51 g (Channel 19) across the span hinge during the Landers èarthquake. This further verified the excellent performance of Route 405/10 Interchange with similar steel jacket retrofit for the single column bent. For that bridge, the peak acceleration recorded at the top of Pier 9 (a 38.5 feet tall column) was 0.52 g in the transverse direction. The measured responses at these two bridges may be considered as the minimum strength of the retrofitted design.

Using the recorded data, additional comparisons were made to benchmark the foundation stiffness calculation procedure typically used in practice. First, it is recognized that most of the foundation flexibility is caused by the rocking of the footing. Secondly, the total deck displacement caused by foundation is predicted to be 7% to 12% which compares very well with the measured data.

It is recognized by several previous research studies that the hinge nonlinear effects, including cable stretching and deck impact, are important. An analytical model is proposed which allows the consideration of energy loss during impact by the restitution coefficient approach. Further studies will be required to calibrate the appropriate restitution coefficient, e, for the various superstructure types.

ACKNOWLEDGMENTS

We acknowledge the funding support of CSMIP and assistance provided by the CSMIP staff to carry out this project. Also, discussions were held with Kelly Horton of Caltrans Division of Structures. She provided valuable photos of the retrofit construction of the Interchange.

REFERENCES

Caltrans (1994), The Northridge Earthquake, Post Earthquake Investigation Report, California Department of Transportation, Division of Structures.

Chai, Y.H. (1996), An Analysis of the Seismic Characteristics of Steel-Jacketed Circular Bridge Columns, Earthquake Engineering and Structural Dynamics, Vol. 25, pp. 149-161.

Cross, W.B. and N.P. Jones (1993), Seismic Performance of Joist-Pocket Connections I: Modeling, Journal of Structural Engineering, ASCE, Vol. 119, No. 10, October.

Fenves, G.L. and R. Desroches (1995), Evaluation of the Response of I-10/215 Interchange Bridge near San Bernardino in the 1992 Landers and Big Bear Earthquakes, Data Utilization Report CSMIP/95-02, March.

Huang, M. et al. (1992), CSMIP Strong-Motion Records from the Big Bear, California Earthquake of June 28, 1992, Report No. OSMS 92-10, California Strong Motion Instrumentation Program, Division of Mines and Geology, August 21, 1992.

Huang, M.J. and A.F. Shakal (1995), CSMIP Strong-Motion Instrumentation Records from the I10/215 Interchange Bridge near San Bernardino, Earthquake Spectra, Vol. 11, No. 2, May 1995.

Housner, G.W. (1994), The Continuing Challenge, The Northridge Earthquake of January 17, 1994, Report to the Director, California Department of Transportation by the Seismic Advisory Board, October.

Imbsen & Associates, Inc. (1991), IAI-NEABS, Integrated Linear and Nonlinear Earthquake Analysis of Bridge Systems and Post Processing Utilities, Sacramento, California, 1991.

Kawashima, and J. Penzien (1976), Correlative Investigation on Theoretical and Experimental Dynamic Behavior of a Model Bridge Structure, Report No. UCB/EERC 76-26, Earthquake Engineering Research Center, University of California, Berkeley.

Liu, W.D. et al. (1994), "Seismic Performance of a Highly Curved Interchange Structure during the 1989 Loma Prieta Earthquake," 5th U.S. National Conference on Earthquake Engineering, Chicago, Illinois, July 1994.

Malhotra, P., M. Huang, and A.F. Shakal (1994), Interaction at Separation Joints of a Concrete Bridge During 1992 Earthquakes in California, Proceedings of the Fifth U.S. National Conference on Earthquake Engineering, Vol. I, pp. 347-256, July 10-14.

Shakal, A. et al. (1994), CSMIP Strong Motion Records from the Northridge, California Earthquake of January 17, 1994, Report No. OSMS 94-07, California Strong Motion Instrumentation Program, Division of Mines and Geology, February 18, 1994.

Shakal, A. et al. (1992), CSMIP Strong-Motion Records from the Landers, California Earthquake of June 28, 1992, Report No. OSMS 92-09, California Strong Motion Instrumentation Program, Division of Mines and Geology, August 5, 1992.

Tseng, W.S., M.S. Yang and J. Penzien (1992), Seismic Performance Investigation of the Hayward BART Elevated Section, Data Utilization Report CSMIP/92-02, California Strong Motion Instrumentation Program, Sep. 1992.

Table 1: San Bernardino Interstate Route 10/215 Interchange – NW Connector Overcrossing – CSMIP Station No. 23631

Sensor #	Motion Direction	Location	A_{max} Landers Earthquake	A_{max} Big Bear Earthquake	A_{max} Northridge Earthquake
1	Longitudinal	Deck, West Abutment 1	0.57g	0.43g	0.15g
2	Vertical	Deck, West Abutment 1	0.20g	0.10g	0.06g
3	Transverse	Deck, West Abutment 1	0.25g	0.19g	0.10g
10	Longitudinal	Deck Hinge Near Bent 3, West Side	0.45g	0.34g	0.15g
7	Transverse	Deck Hinge Near Bent 3, West Side	0.36g	0.38g	0.17g
8	Transverse	Deck Hinge Near Bent 3, East Side	0.59g	0.48g	0.18g
4	Longitudinal	Footing, Bent 3	0.10g	0.09g	0.06g
6	Transverse	Footing, Bent 3	0.10g	0.11g	0.10g
11	Transverse	Deck between Bents 5 & 6, Mid-Span	0.39g	0.28g	0.12g
9	Vertical	Deck, Bent 7	0.21g	0.17g	0.11g
14	Vertical	Deck between Bents 7 & 8, Mid-Span	0.36g	0.31g	0.20g
15	Vertical	Deck Hinge Near Bent 8, North Side	0.35g	0.32g	0.16g
16	Vertical	Deck Hinge Near Bent 8, South Side	0.45g	0.33g	0.18g
12	Vertical	Deck, Bent 8, North Side	0.26g	0.21g	0.13g
13	Vertical	Deck, Bent 8, South Side	0.38g	0.23g	0.31g
5	Vertical	Footing, Bent 8, North Side	0.11g	0.08g	0.03g
23	Vertical	Footing, Bent 8, South Side	0.07g	0.08g	0.04g
17	Longitudinal	Deck Hinge Near Bent 8, West Side	0.66g	0.34g	0.08g
18	Longitudinal	Deck Hinge Near Bent 8, East Side	0.71g	0.58g	0.08g
22	Longitudinal	Footing, Bent 8, South Side	0.17g	0.25g	0.08g
19	Transverse	Deck Hinge Near Bent 8, West Side	0.51g	0.51g	0.16g
20	Transverse	Deck Hinge Near Bent 8, East Side	0.39g	0.33g	0.15g
24	Transverse	Footing, Bent 8, South Side	0.18g	0.15g	0.13g
25	Transverse	Deck Hinge Near Bent 10, West Side	0.33g	0.29g	0.14g
26	Transverse	Deck Hinge Near Bent 10, East Side	0.31g	0.25g	0.15g
28	Longitudinal	Deck Hinge Near Bent 11, West Side	0.29g	0.42g	0.12g
33	Longitudinal	Deck Hinge Near Bent 11, East Side	0.82g	0.68g	0.09g
29	Transverse	Deck Hinge Near Bent 11, West Side	0.29g	0.30g	0.18g
30	Transverse	Deck Hinge Near Bent 11, East Side	0.43g	0.41g	0.26g
31	Transverse	Deck Hinge Near Bent 14, West Side	0.36g	1.02g	0.47g
32	Transverse	Deck Hinge Near Bent 14, East Side	0.47g	0.67g	0.31g
34	Longitudinal	Deck, North Abutment 17	0.36g	0.23g	0.16g
35	Vertical	Deck, North Abutment 17	0.13g	0.11g	0.05g
36	Transverse	Deck, North Abutment 17	0.15g	0.20g	0.14g

Table 2: Interstate Route 10/215 Interchange Sensor Locations by Frame

Structure Frame	Direction*	Sensor ID	
		Deck	Foundation
1 Abutment 1 to Hinge 1 (Bents 2 and 3)	L	10	1, 4
	T	7	3, 6
	V	–	2
2 Hinge 1 to Hinge 2 (Bents 4, 5, 6 and 7)	L	17	–
	T	8, 11, 19	–
	V	9, 14, 15, 16	–
3 Hinge 2 to Hinge 3 (Bents 8 and 9)	L	18	22
	T	20, 25	24
	V	12, 13	5, 23
4 Hinge 3 to Hinge 4 (Bents 10 and 11)	L	28	–
	T	26,29	–
	V	–	–
5 Hinge 4 to Hinge 5 (Bents 12 and 13)	L	33	–
	T	30, 31	–
	V	–	–
6 Hinge 6 to Abutment 17 (Bents 14, 15 and 16)	L	–	34
	T	32	36
	V	–	35

* L: Longitudinal
T: Transverse
V: Vertical

Table 3: Summary of Free Field Spectral Acceleration

	PGA	T = 0.5 sec.	T = 1.5 sec.
Longitudinal			
Landers	0.08 g	0.25 g	0.10 g
Big Bear	0.05 g	0.18 g	0.15 g
Northridge	0.08 g	0.16 g	0.02 g
Transverse			
Landers	0.08 g	0.22 g	0.30 g
Beg Bear	0.11 g	0.18 g	0.15 g
Northridge	0.07 g	0.38 g	0.02 g

Table 4: Column Stiffness, Damping and Foundation Effect at Bent 8

	f_{FB} (Hz)	ξ	k (kip/ft)	u_{max} (inch)	$1+\frac{k}{\bar{k}}$
Landers EQ	0.73	3.9%	1942	5.60	1.07
Big Bear EQ	0.83	4.4%	2511	3.50	1.09
Northridge EQ	0.96	4.1%	3359	1.25	1.12

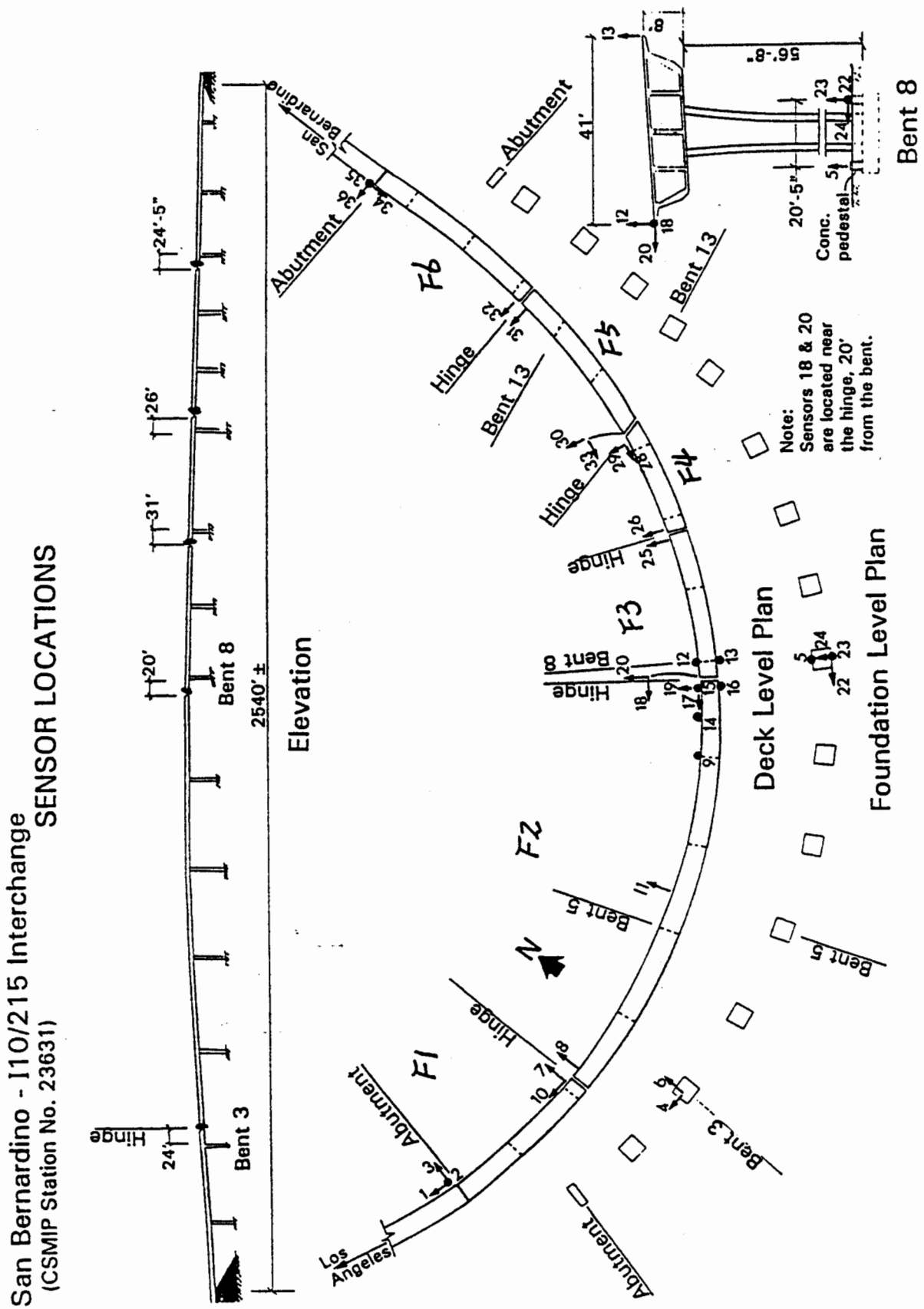

Figure 1: Plan, Elevation and Instrumentation Locations of the NW Connector in the I10/215 Interchange

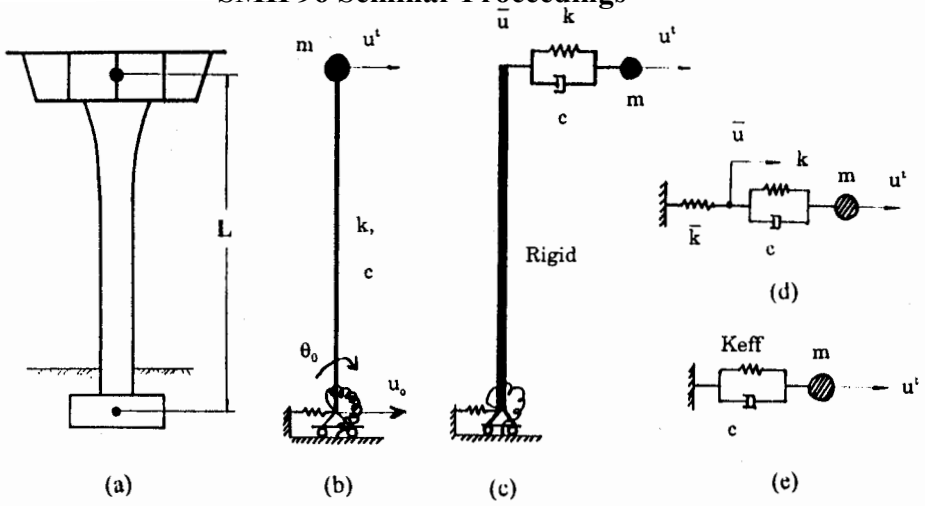

Figure 2: Idealization of a Single Column Bent

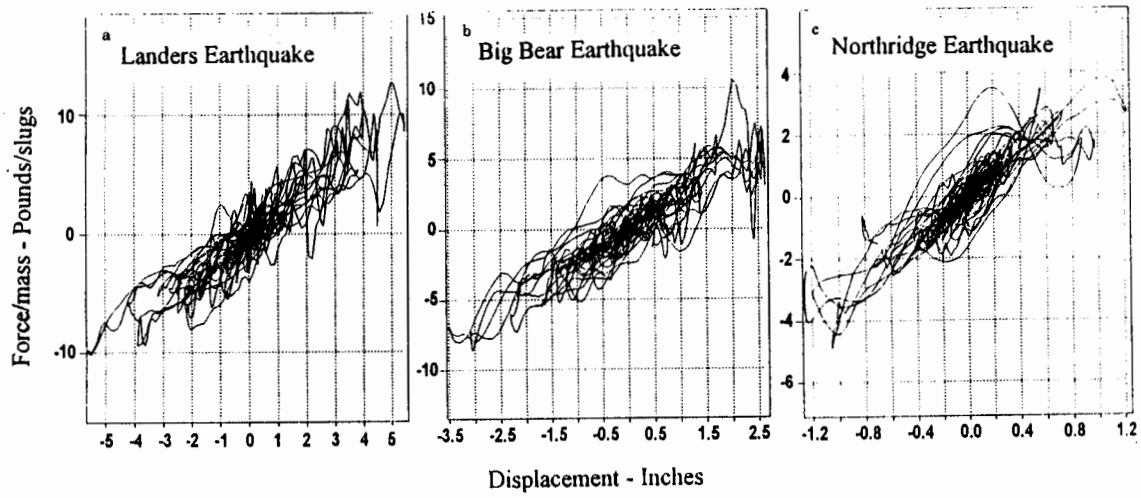

Figure 3: Normalized Force-Displacement Hysteresis Loop for the Transverse Response of Bent 8

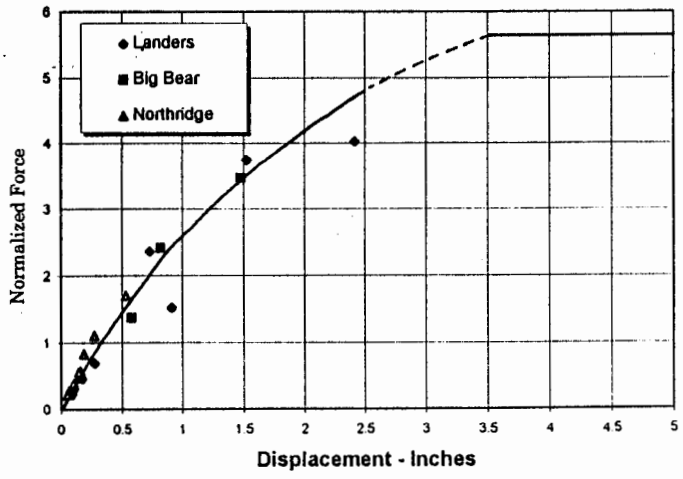

Figure 4: Nonlinear Force-Displacement Relation Based on RMS Force-Displacement Pairs from Measured Data

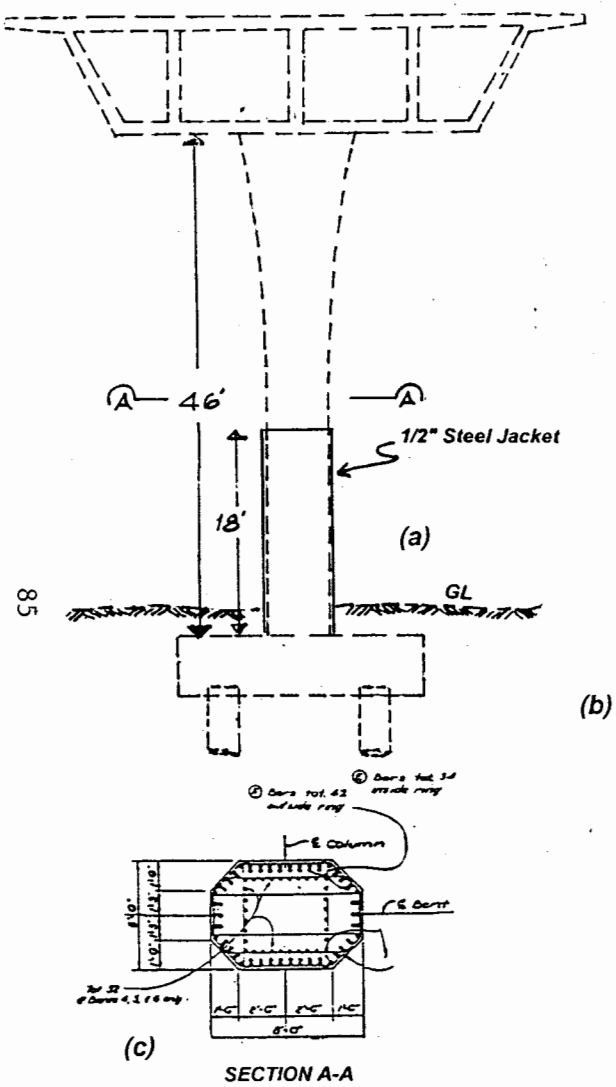

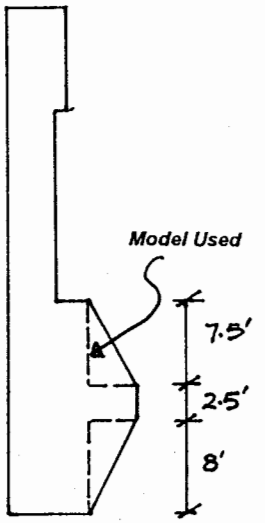

(b) Variation of Effective (EI) Along Column Height

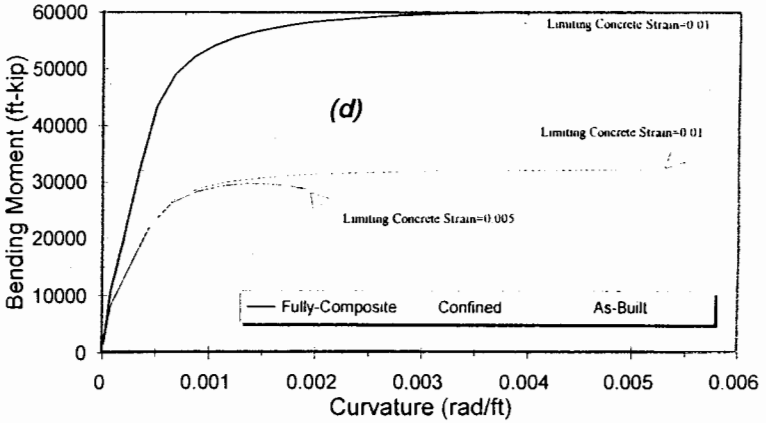

(d) M-ψ Relationships

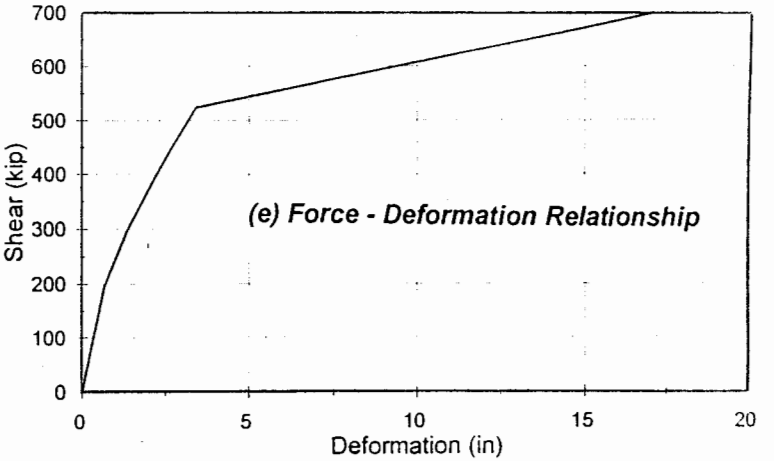

Figure 5: Component Behavior Characterization of the Retrofitted Column

Impact of Adjacent Frames

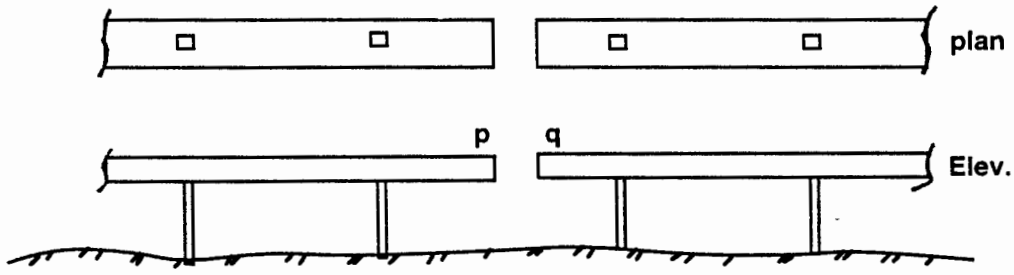

a. Before Impact

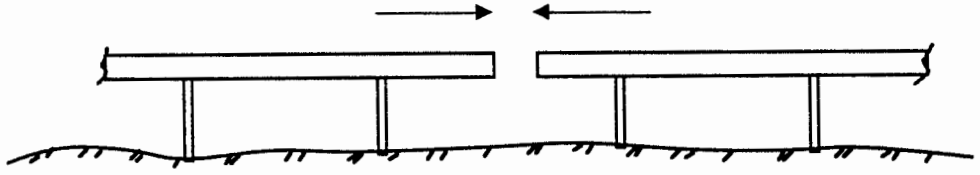

b. During Impact

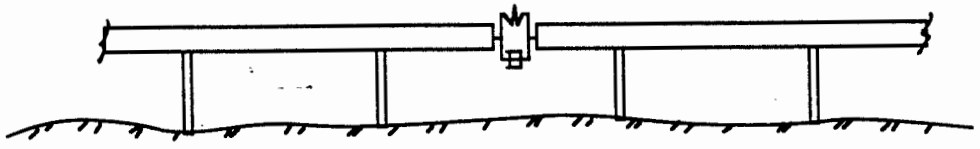

c. After Impact

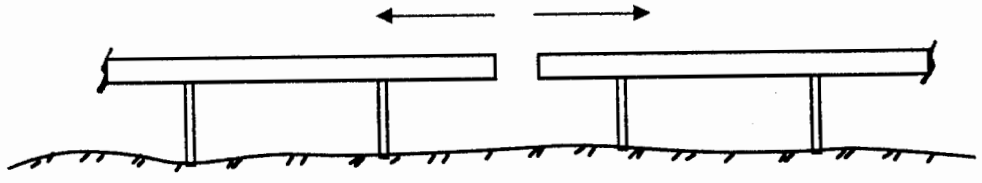

Figure 6: Modeling of Impact between Adjacent Frames

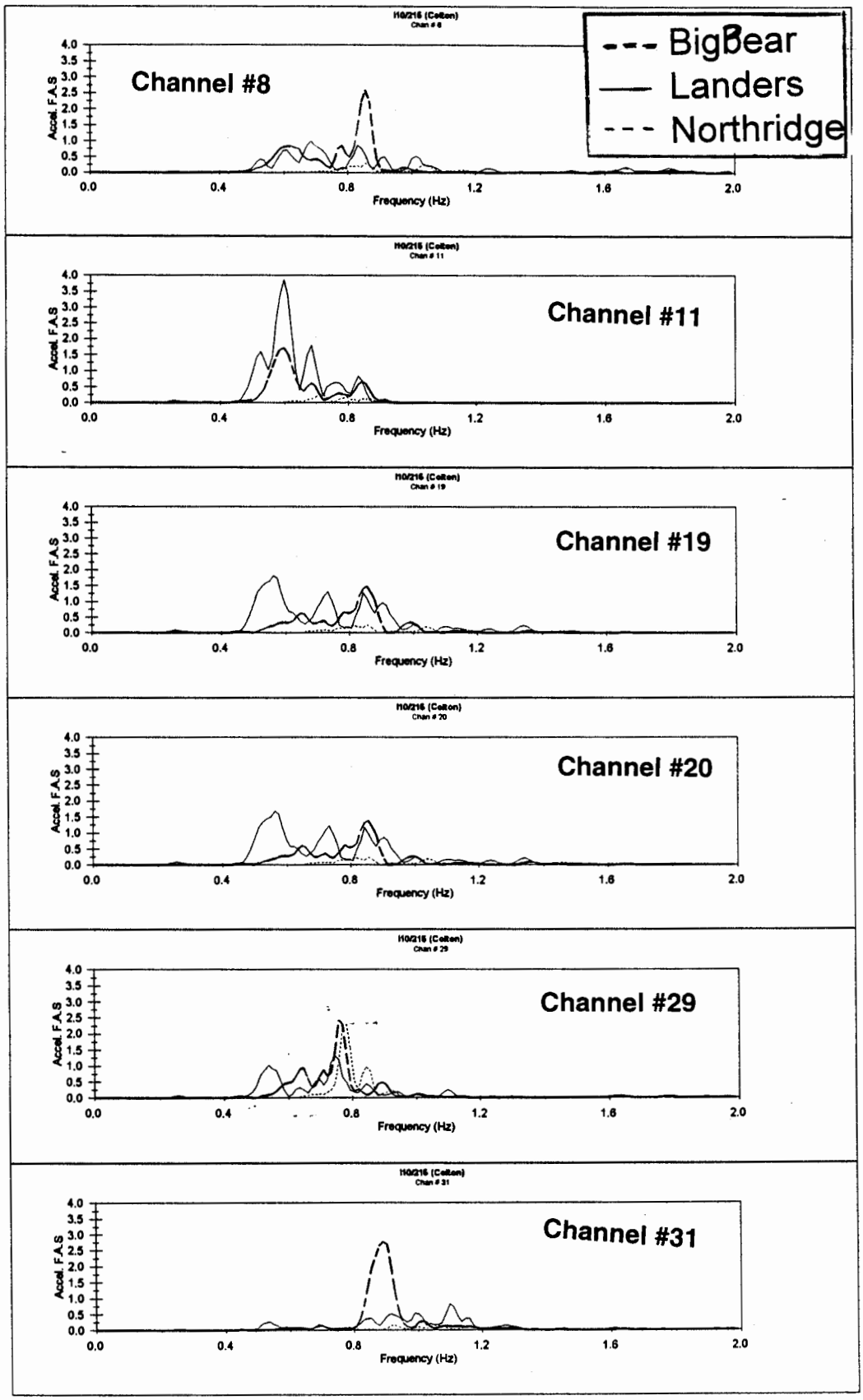

Figure 7: Fourier Amplitude Spectra for the Three Earthquakes

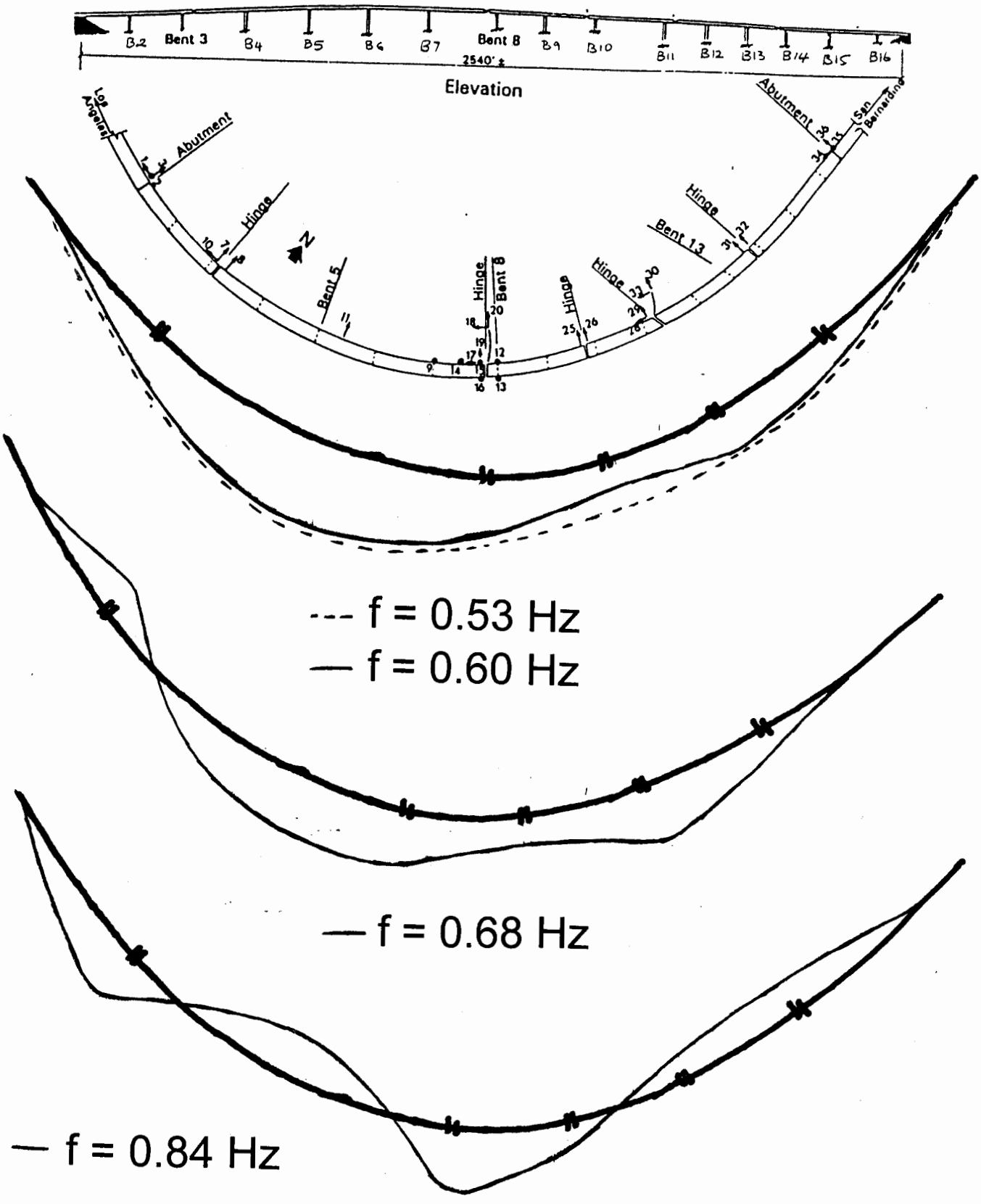

Figure 8: Dominant Vibration Mode Shapes